Improving the hydrogen cycling properties by Mg addition in Ti-V-Zr-Nb refractory high entropy alloy

Jorge Montero, Gustav Ek, Martin Sahlberg, Claudia Zlotea

Improving the hydrogen cycling properties by Mg addition in Ti-V-Zr-Nb refractory high entropy alloy

Jorge Montero[1], Gustav Ek[2], Martin Sahlberg[2], Claudia Zlotea[1*]

[1]*Univ Paris Est Créteil, CNRS, ICMPE, UMR 7182, 2 rue Henri Dunant, 94320 Thiais, France*

[2]*Department of Chemistry - Ångström Laboratory, Uppsala University, Box 523, SE-75120 Uppsala, Sweden*

* Corresponding author: claudia.zlotea@icmpe.cnrs.fr

Abstract (150 words)

A novel high entropy alloy containing Mg and refractory elements has been prepared by mechanochemical synthetic method under inert atmosphere. The $Mg_{0.10}Ti_{0.30}V_{0.25}Zr_{0.10}Nb_{0.25}$ alloy adopts a single-phase bcc lattice and can absorb hydrogen within 1 minute at room temperature forming a hydride phase with 1.7 H/M (2.7 wt.%) capacity. During the reaction with hydrogen the alloy undergoes a single-step and reversible phase transformation from bcc (alloy) to fcc lattice (hydride). The absorption/desorption cycling properties prove a small fading of the capacity for the first cycle followed by stabilization to 1.5 H/M (2.4 wt.%) for the next cycles. A simple comparison between this quinary HEA and the quaternary alloy containing only refractory elements $Ti_{0.325}V_{0.275}Zr_{0.125}Nb_{0.275}$ proves an important enhancement of the cycling properties by Mg addition. These insights seem to suggest that insertion of light-weighted metals such as, Mg, can guide future design of novel HEA with improved performances for hydrogen storage.

Keywords: high entropy alloys, hydrogen absorption/desorption cycling, synchrotron-XRD, in situ neutron diffraction

In contrast with conventional alloys based on one or two elements with minor substitutions, high entropy alloys (HEA) comprise multiprincipal elements close to equimolar composition, *i.e.* at least five elements with concentration between 5 and 35 at.% [1–3]. The large configuration entropy of mixing of these alloys has been suggested to stabilize single-phased disordered solid solutions. The crystalline structure of these alloys often adopts simple lattices such as, body centered cubic (bcc), face centered cubic (fcc) or hexagonal close compact (hcp). Consequently, the elements are randomly distributed on a single crystallographic site, which introduces large lattice distortion. This effect is often quantified within the HEA community as the δ parameter, which describes a distorted crystal lattice due to the mixing of many metals with different atomic radii (as defined in reference [1]).

Several reports on the hydrogen storage properties of refractory HEAs have been recently published and some compositions possess remarkable hydrogen storage capacities [4–6]. For example, the equimolar TiVZrNbHf has been shown to absorb hydrogen up to 2.5 hydrogen per metal (H/M), which is greater than the capacity of each individual element (2 H/M) [4]. Recently, several compositions with interesting hydrogen absorption properties have been proposed but they contain exclusively refractory elements [7–11]. Most of these alloys are single-phased bcc solid solutions with a maximum hydrogen capacity close to 2.0 H/M. However, their gravimetric capacity is modest due to the presence of rather heavy metals (4d and 5d transition metals).

Efficient hydrogen storage requires the use of light-weighted materials to increase the gravimetric capacity. Several attempts have been reported for producing HEAs containing light elements, such as, Mg, with limited success in terms of hydrogen uptake [12–15]. Moreover, Mg is one of the most studied metals for hydrogen storage due to the high capacity of MgH_2 (7.6 wt.%), high abundancy and low cost of production. Zepon *et al*. synthesized $MgZrTiFe_{0.5}Co_{0.5}Ni_{0.5}$ using high-energy ball milling under Ar atmosphere [12]. This alloy is a

single-phased solid solution with bcc lattice and a maximum capacity of 1.2 wt% (0.7 H/M) at relatively high temperature. The authors also directly synthesized the corresponding HEA hydride by reactive ball milling (RBM) under hydrogen pressure. The same group has recently reported a new A_2B type HEA $Mg_{0.68}TiNbNi_{0.55}$ with a capacity of around 1.6 wt.% [14]. Recently, de Marco *et al*. prepared MgTiVCrFe high entropy alloy by high-energy ball milling under hydrogen atmosphere followed by high-pressure torsion processing to improve activation [13]. However, the latter composition showed low affinity to hydrogen as well as partial decomposition by hydrogen absorption/desorption cycling. Another study focused on bcc equimolar MgVAlCrNi HEA but its capacity was found very low (~ 0.3 wt.%) [15].

Despite recent research efforts in the topic of HEAs for hydrogen storage, Mg containing HEAs are very scarcely reported. In this context, the present study reports on the preparation of a novel $Mg_{0.10}Ti_{0.30}V_{0.25}Zr_{0.10}Nb_{0.25}$ high entropy alloy together with the characterisation of the structural and hydrogen sorption properties. Our strategy is to highlight the effect of the addition of Mg into the quaternary alloy $Ti_{0.325}V_{0.275}Zr_{0.125}Nb_{0.275}$ with optimized composition, as reported previously [7].

Due to the low melting temperature and high vapour pressure of Mg, classical melting techniques are not appropriate for the preparation of Mg-containing alloys. Therefore, the $Mg_{0.10}Ti_{0.30}V_{0.25}Zr_{0.10}Nb_{0.25}$ alloy was synthesized by high-energy ball milling under Ar atmosphere starting from pure elemental powders, as described earlier [7]. The milling process was conducted for a total of 2 hours. Another approach was to directly prepare the hydride phase with the same metal composition by RBM under 70 bar H_2 pressure for 1 hour, as detailed previously [7,8]. Both alloy and hydride phases were manipulated and stored in the glove box due to their pyrophoricity.

The hydrogen storage properties, *i.e.* pressure–composition isotherms (PCI) and kinetic curves at room temperature together with absorption/desorption cycling were measured by using a home-made volumetric instrument. The alloy in the form of fine powder was loaded without air exposure and activated by heating under dynamic vacuum at 340 °C for 2 hours.

The hydrogen desorption properties have been studied by thermal desorption spectroscopy (TDS) using a home-made instrument, as described in a previous report [16]. The sample was loaded without air exposure and the hydrogen desorption profile was measured by the help of a quadrupole mass spectrometer during heating with a constant rate of 1 °C/min.

The crystalline structure of the samples was studied by powder X-ray diffraction (XRD) using both laboratory and synchrotron sources. Laboratory investigations (XRD) have been performed by the help of a D8 advance Bruker diffractometer (Cu Kα radiation, Bragg-Brentano Geometry). Synchrotron XRD measurements (SR-XRD) were carried out at the Cristal beamline in SOLEIL facility (Debye-Scherrer geometry with λ = 0.72896 Å). A capillary tube of 0.2 mm of diameter was filled with finely grounded powder. The acquisition time was approximately 10 minutes for a scanning range from 1° to 85° (2θ).

Powder neutron diffraction experiments on deuteride samples were performed on the D1B beamline at the Institute Laue-Langevin with λ = 1.28 Å in the scanning range from 1 to 128° (2θ). Both ex situ and in situ measurements were performed using a vanadium container and a silica tube, respectively. The silica tube containing the powder sample was connected to secondary vacuum during desorption while constant heating with 1 °C/min. The pressure of evolved gas was continuously recorded during the desorption experiment with the help of a vacuum gauge.

The crystalline structure of the alloys/hydrides/deuterides was determined by Rietveld analysis using the software Fullprof on both X-ray and neutron diffraction patterns.

The microstructure was studied by scanning electron microscopy (SEM) using a Zeiss Merlin microscope complemented by energy dispersive spectroscopy (EDS) from Oxford Instruments. Powder samples were immobilized in epoxy resin and coated with 1-2 nm of Pd. A chemical mapping was performed on the samples after the first and last hydrogen absorption/desorption cycle to determine the chemical homogeneity change and eventual phase separation.

The $Mg_{0.10}Ti_{0.30}V_{0.25}Zr_{0.10}Nb_{0.25}$ alloy is a single-phase material with bcc lattice, as proven by the XRD and related Rietveld analysis in Fig 1-A. The diffraction peaks are broad due to the ball-milling process which is well known to refine the crystallite size and to introduce defects into the structure. The lattice parameter a = 3.273 (1) Å (Table 1) is slightly larger than the quaternary $Ti_{0.325}V_{0.275}Zr_{0.125}Nb_{0.275}$ alloy a = 3.270 (1) Å synthesized by the same method, as reported earlier [7]. The lattice distortion for the quinary alloy δ = 6.6 % is a little higher than 6.0 % for the quaternary composition without Mg. These effects can be understood by the largest atomic size of Mg (1.60 Å) as compared to other metals in the composition (1.31, 1.43, 1.45 and 1.59 Å for V, Nb, Ti and Zr, respectively [17]).

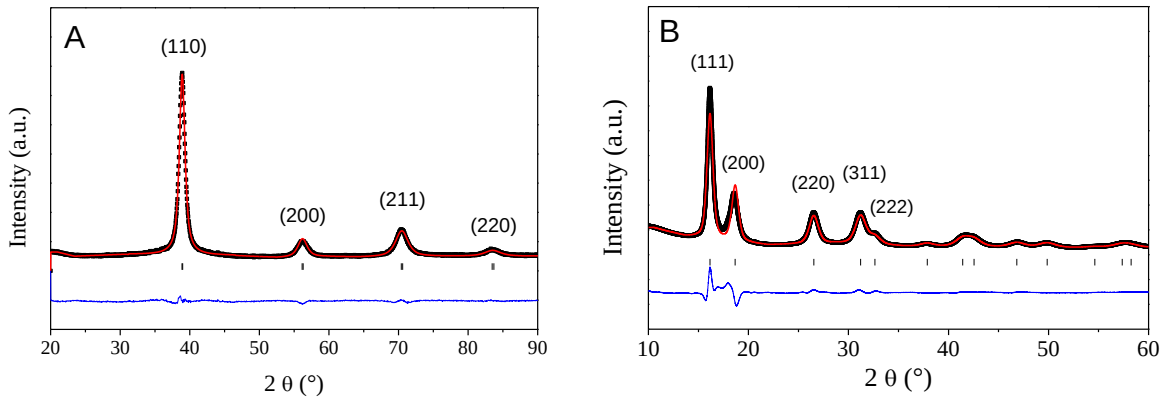

Fig 1. XRD pattern (λ = 1.5406 Å) of the ball milled $Mg_{0.10}Ti_{0.30}V_{0.25}Zr_{0.10}Nb_{0.25}$ alloy and related Rietveld analysis (A) and SR-XRD pattern (λ = 0.72896 Å) of the hydride $Mg_{0.10}Ti_{0.30}V_{0.25}Zr_{0.10}Nb_{0.25}H_{1.7}$ and related Rietveld analysis (B).

Sample	Synthesis	State	H content	Lattice	a (Å)
$Mg_{0.10}Ti_{0.30}V_{0.25}Zr_{0.10}Nb_{0.25}$	BM	As-prepared	-	bcc	3.273(1)
$Mg_{0.10}Ti_{0.30}V_{0.25}Zr_{0.10}Nb_{0.25}H_{1.72}$	BM	1st cycle absorption	1.72 H/M 2.70 wt.%	fcc	4.492(1)
$Mg_{0.10}Ti_{0.30}V_{0.25}Zr_{0.10}Nb_{0.25}H_{1.5}$	BM	12th cycle absorption	1.53 H/M 2.41 wt.%	fcc	4.498(1)
$Mg_{0.10}Ti_{0.30}V_{0.25}Zr_{0.10}Nb_{0.25}H_{1.65}$	RBM	As-prepared	1.65 H/M 2.60 wt.%	fcc	4.504(1)
$Ti_{0.325}V_{0.275}Zr_{0.125}Nb_{0.275}$[7]	BM	As-prepared	-	bcc	3.270(1)
$Ti_{0.325}V_{0.275}Zr_{0.125}Nb_{0.275}H_{1.8}$	RBM	As-prepared	1.80 H/M 2.63 wt.%	fcc	4.497(1)

Table 1. Structural properties of $Mg_{0.10}Ti_{0.30}V_{0.25}Zr_{0.10}Nb_{0.25}$ and $Ti_{0.325}V_{0.275}Zr_{0.125}Nb_{0.275}$ alloys obtained by ball milling under inert atmosphere (BM) or under hydrogen pressure (RBM) and related hydride/cycled phases.

The hydrogen absorption properties have been first tested by measuring a kinetic curve at 25 °C under a final equilibrium pressure of 25 bar (Fig 2 - A). The alloy rapidly absorbs hydrogen at room temperature, reaching a maximum capacity of 1.72 H/M (2.70 wt.%) within 1 minute. The kinetics of absorption are very fast in the quinary alloy while the $Ti_{0.325}V_{0.275}Zr_{0.125}Nb_{0.275}$ alloy reaches full capacity only after 40 minutes (see Fig SI-1).

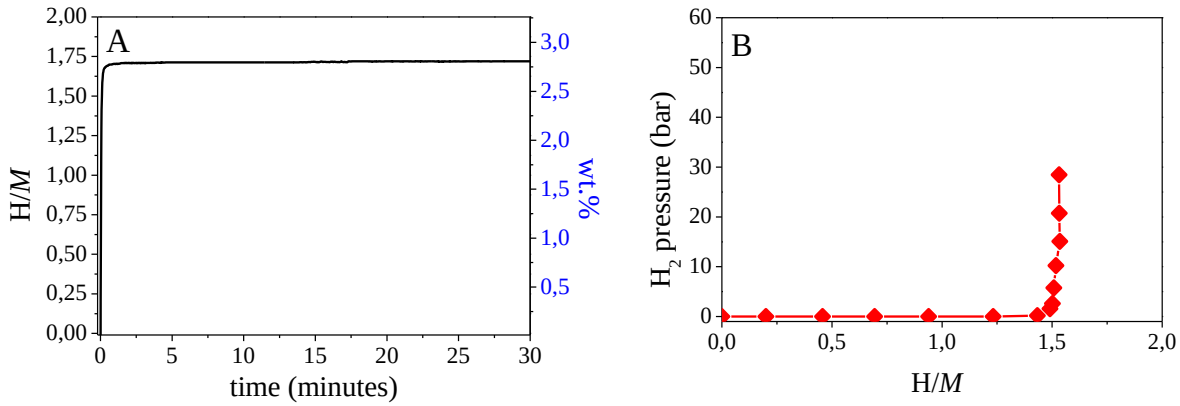

Fig 2. Kinetics of absorption at 25 °C for a final equilibrium pressure of 25 bar – first hydrogenation (A) and Pressure-Composition-Isotherm at 25 °C – second hydrogenation (B).

After hydrogen desorption from the hydride obtained in the first hydrogenation test, a PCI curve was measured at room temperature (Fig 2-B) and shows a single plateau at low equilibrium pressure, as also noticed for the quaternary counterpart [7]. The maximum capacity of the PCI curve is 1.53 H/M (2.41 wt.%), which is slightly smaller than the initial value obtained for the kinetic curve at the same temperature. The observed fading of the capacity during cycling will be addressed later.

The hydride phase adopts a fcc lattice with the parameter a = 4.492(1) Å (Table 1), as characterized by SR-XRD (Fig 1-B). Moreover, the fcc hydride phase with almost the same capacity (1.65 H/M) and slightly larger lattice parameter (4.504(1) Å) could be directly prepared by RBM under 70 bar H_2 after only 1 hour of process (Table 1 and Fig SI-2). The lattice parameter of the RBM hydride phase is slightly greater than the corresponding quaternary hydride (4.497(1) Å) synthesized by the same process (Table 1 and Fig SI-3).

The hydrogen (deuterium) was localized in the tetrahedral sites of the fcc lattice (CaF_2 type structure) by ex situ neutron diffraction on a deuterated sample with maximum capacity 1.72 D/M. The neutron diffraction pattern and corresponding Rietveld refinement are shown in Fig SI-4. This result is in good agreement with previous findings in the literature in similar refractory HEAs.[6,8]

The desorption properties have been determined by TDS and in situ neutron diffraction under dynamic vacuum with a constant temperature rate of 1 °C/min (Fig 3).

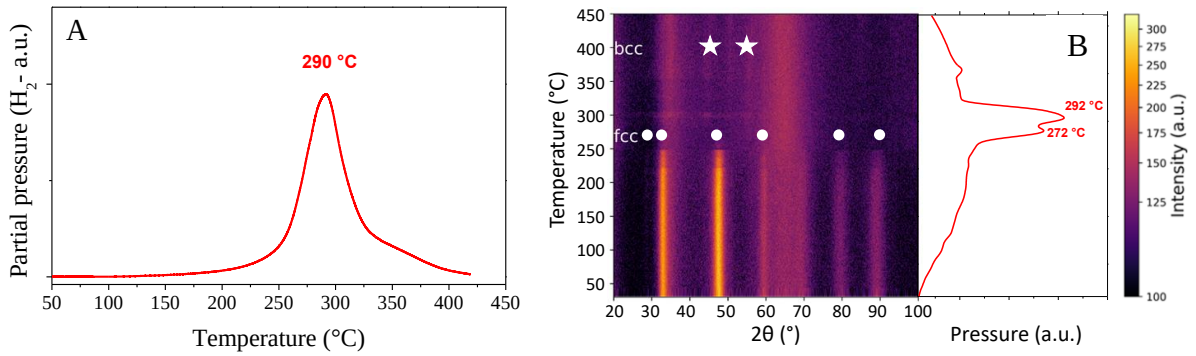

Fig 3. TDS profile for the hydrogen desorption from $Mg_{0.10}Ti_{0.30}V_{0.25}Zr_{0.10}Nb_{0.25}H_{1.72}$ with 1 °C/min (A) and in situ neutron diffraction of $Mg_{0.10}Ti_{0.30}V_{0.25}Zr_{0.10}Nb_{0.25}D_{1.7}$ (λ = 1.28 Å) together with the vacuum pressure reading during constant heating up to 450 °C with 1°C/min under dynamic vacuum (B).

The hydrogen desorption from the $Mg_{0.10}Ti_{0.30}V_{0.25}Zr_{0.10}Nb_{0.25}H_{1.72}$ occurs within a single step (one desorption peak in Fig 1-A) with an onset temperature at around 250 °C and a maximum desorption rate at 290 °C, in agreement with the vacuum pressure reading during in situ neutron diffraction (Fig 3-B right).

Thermo-diffraction patterns (Fig 3-B) clearly show diffraction signals from two phases: the fcc hydride (circle) and the silica tube used as sample holder as the broad peaks at 2θ around 32-36° and 60-70°. Starting from the bottom to the top, the intensity of the signal of the fcc phase seems to smoothly decrease up to ~250 °C. This can be understood by small deuterium desorption in agreement with the increasing pressure profile on the right of Fig 3-B. After 250 °C the fcc diffraction peaks completely disappear, which indicates full deuterium desorption, in agreement with the maximum desorption event in the desorption profile. At high temperature, few very low-intensity peaks in between 40 and 60° can be noticed (stars). Based on our previous study, we can hypothesize that the very small diffraction peaks marked with stars above 350 °C can be attributed to the desorbed bcc phase [8]. Moreover, we can observe that the diffraction peaks of the desorbed alloy are very weak as compared to the deuteride phase due to the low thermal neutron cross-section of the alloy. It has been already reported that refractory high entropy alloys are highly transparent to thermal neutron beam [4] and thus,

interesting candidates as cladding materials for nuclear reactors [18]. Therefore, these experiments proven that the hydrogen absorption and desorption reactions are fully reversible and occur within a single-step transformation from bcc ↔ fcc, as also proposed for the quaternary alloy [7].

It is worth to compare the desorption properties of the quinary alloy with the pristine quaternary composition (BM), as already reported elsewhere [7]. The quaternary alloy shows one main desorption peak at around 330 °C followed by a second event above 400 °C (see figure 5 in reference [7]). Thus, the addition of 10 % Mg in the pristine quaternary alloy improves the desorption kinetics by changing the TDS profile from two to one main thermal event and decreasing the temperature of desorption below 300 °C.

After defining the desorption conditions (heating to maximum 400 °C under dynamic vacuum), hydrogen absorption/desorption cycling properties were determined and compared to the quaternary alloy also prepared by mechanochemical synthesis, as reported previously [7] (Fig 4). The absorption was performed at room temperature under a final equilibrium pressure of 25 bar, whereas the desorption was carried out by heating at 400 °C under dynamic vacuum for 10 hours.

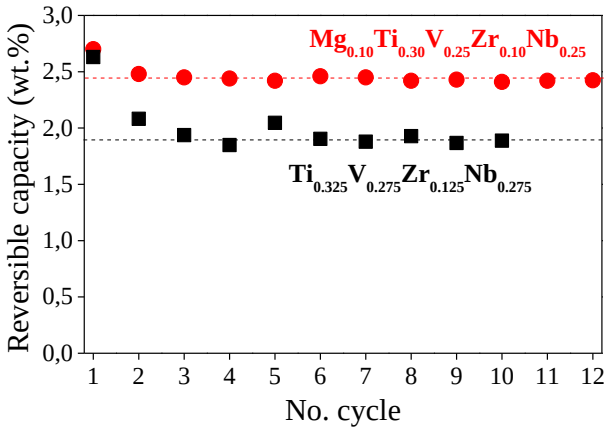

Fig 4. Comparison between the variation of the reversible hydrogen storage capacity during absorption/desorption cycling for the quinary $Mg_{0.10}Ti_{0.30}V_{0.25}Zr_{0.10}Nb_{0.25}$ and quaternary $Ti_{0.325}V_{0.275}Zr_{0.125}Nb_{0.275}$ alloys.

The quinary alloy loses around 11 % capacity (from 2.70 to 2.41 wt. %) in the second cycle followed by a stabilization of the reversible capacity to approximately 2.4 wt.% for the subsequent cycles. This fast stabilization is in contrast with the quaternary alloy that progressively loses nearly 28 % of capacity during the first 4 cycles before reaching a stable value around 1.9 wt.%. Obviously, the Mg containing HEA possesses a larger reversible capacity than the corresponding quaternary HEA (without Mg). Moreover, the value of the reversible capacity (2.4 wt.%) is better than other classical intermetallics such as, $LaNi_5$ (1.5 wt.%), YFe_3 (1.9 wt.%), TiFe (1.9 wt.%) [19] and other bcc Ti-V-Cr alloys (1.5 wt.%) [20].

Furthermore, the cycling of the quinary alloy does not induce any phase segregation, as characterized by XRD (Fig SI-5) and SEM-EDS (Fig SI-6). The crystalline structures after 12 cycles are maintained (bcc for the desorbed phase and fcc for the hydride) with very similar lattice parameters (Table 1). The chemical mapping after 1^{st} and 12^{th} cycles proven that the chemical composition is close to the nominal one (~ 1 at. % error) and the distribution of elements is homogenous without phase segregation. Additionally, no obvious change in the TDS profile after cycling could be observed (Fig SI-7) indicating a very stable behavior during cycling.

Consequently, despite many similarities between the quaternary and the quinary alloys such as, very close chemical composition, with only 10 at.% change by addition of Mg, same lattices for initial/desorbed (bcc) and hydride (fcc) phases, same reversible phase transformation during reaction with hydrogen (bcc $\leftrightarrow$ fcc), the quinary $Mg_{0.10}Ti_{0.30}V_{0.25}Zr_{0.10}Nb_{0.25}$ alloy demonstrated better cycling properties relative to the quaternary alloy $Ti_{0.325}V_{0.275}Zr_{0.125}Nb_{0.275}$. The quinary HEA has a larger stable capacity of nearly 2.4 wt.% and faster stabilisation than the quaternary counterpart.

Fading capacity during first absorption/desorption cycles is a widely observed phenomenon in metal hydrides (classical bcc, intermetallics, and multi-principal element alloys).[21,22] Both extrinsic or intrinsic factors have be invoked for explaining this feature. The most well-known extrinsic factors are the impurities in the H_2 gas or the vacuum contaminants that can poison the alloy's surface by either oxidation or adsorption of hydrocarbons and consequently, degrade the reversible capacity. Among the intrinsic factors we can mention the disproportionation *via* the formation of thermodynamically stable monohydride phases of individual components (TiH_2, VH_2…), the inhomogeneities in the chemical composition, the kinetics issues that may lead to incomplete absorption or desorption and the decrease in the degree of crystallinity …

Our comparative study is done under the same experimental conditions therefore, the extrinsic factors are expected to affect similarly both quinary and quaternary alloys. Thus, we suggest that intrinsic factors might be responsible for the differences in the cycling performances rather than extrinsic ones. We hypothesize that the very good homogeneity of the quinary Mg-alloy might be responsible for the better cycling properties relative to the quaternary composition through an enhancement of the kinetics of both absorption and desorption reactions, as exposed above. Improved chemical homogeneity has been already proposer earlier as key factor for the stability of cycling in bcc alloys [22]. The latter study reported that small carbon doping in a TiVCr bcc alloy increases the chemical homogeneity and suppresses the microstructural segregation which, subsequently, improves the cycling stability. Due the complexity of our materials, precise characterization techniques would be necessary to properly address this issue, for example, total scattering paired with PDF analysis, as proposed recently [10]. However, this is beyond the scope of this report.

In conclusions, these insights demonstrated that the insertion of light-weighted metals such as, Mg, into refractory HEAs is beneficial for improving the reversibility of hydrogen absorption/desorption cycling. Due to the endless possibility to explore the compositional space

of these alloys, this finding can guide future design of novel HEAs with improved performances for hydrogen storage.

Acknowledgments

We acknowledge ILL for beamtime allocation on the CRG-D1B beamline. Laetitia Laversenne, Vivian Nassif from Institut Néel, CNRS Grenoble and Fabrice Couturas from ICMPE are acknowledged for help with neutron diffraction at ILL. Eric Elkaim from SOLEIL and Benoit Baptiste from IMPMC CNRS are thanked for their help with synchrotron radiation exepriments at SOLEIL. CZ acknowledge the French National Research Agency (ANR) for the financial support for the MASSHY project (ANR-19-CE05-0029-01). MS and GE acknowledge financial support from the NordForsk Nordic Neutron Science Programme through the Functional hydrides (FunHy) project (grant number 81942).

References

[1] Y.F. Ye, Q. Wang, J. Lu, C.T. Liu, Y. Yang, Materials Today 19 (2016) 349–362.
[2] D.B. Miracle, O.N. Senkov, Acta Materialia 122 (2017) 448–511.
[3] D.B. Miracle, Nature Communications 10 (2019) 1805.
[4] M. Sahlberg, D. Karlsson, C. Zlotea, U. Jansson, Scientific Reports 6 (2016) 36770.
[5] L.J. Bannenberg, M. Heere, H. Benzidi, J. Montero, E.M. Dematteis, S. Suwarno, T. Jaroń, M. Winny, P.A. Orłowski, W. Wegner, A. Starobrat, K.J. Fijałkowski, W. Grochala, Z. Qian, J.-P. Bonnet, I. Nuta, W. Lohstroh, C. Zlotea, O. Mounkachi, F. Cuevas, C. Chatillon, M. Latroche, M. Fichtner, M. Baricco, B.C. Hauback, A. El Kharbachi, International Journal of Hydrogen Energy (2020).
[6] D. Karlsson, G. Ek, J. Cedervall, C. Zlotea, K.T. Møller, T.C. Hansen, J. Bednarčík, M. Paskevicius, M.H. Sørby, T.R. Jensen, U. Jansson, M. Sahlberg, Inorg. Chem. 57 (2018) 2103–2110.
[7] J. Montero, C. Zlotea, G. Ek, J.-C. Crivello, L. Laversenne, M. Sahlberg, Molecules (2019) 2799.
[8] J. Montero, G. Ek, L. Laversenne, V. Nassif, G. Zepon, M. Sahlberg, C. Zlotea, Journal of Alloys and Compounds 835 (2020) 155376.
[9] M.M. Nygård, G. Ek, D. Karlsson, M. Sahlberg, M.H. Sørby, B.C. Hauback, International Journal of Hydrogen Energy (2019).
[10] M.M. Nygård, W.A. Sławiński, G. Ek, M.H. Sørby, M. Sahlberg, D.A. Keen, B.C. Hauback, Acta Materialia (2020).

[11] C. Zlotea, M.A. Sow, G. Ek, J.-P. Couzinié, L. Perrière, I. Guillot, J. Bourgon, K.T. Møller, T.R. Jensen, E. Akiba, M. Sahlberg, Journal of Alloys and Compounds 775 (2019) 667–674.
[12] G. Zepon, D.R. Leiva, R.B. Strozi, A. Bedoch, S.J.A. Figueroa, T.T. Ishikawa, W.J. Botta, International Journal of Hydrogen Energy 43 (2018) 1702–1708.
[13] M.O. de Marco, Y. Li, H.-W. Li, K. Edalati, R. Floriano, Advanced Engineering Materials n/a (2019) 1901079.
[14] F. Marques, H.C. Pinto, S.J.A. Figueroa, F. Winkelmann, M. Felderhoff, W.J. Botta, G. Zepon, International Journal of Hydrogen Energy 45 (2020) 19539–19552.
[15] R.B. Strozi, D.R. Leiva, J. Huot, W.J. Botta, G. Zepon, International Journal of Hydrogen Energy (2020).
[16] C. Zlotea, Y. Oumellal, M. Msakni, J. Bourgon, S. Bastide, C. Cachet-Vivier, M. Latroche, Nano Letters 15 (2015) 4752–4757.
[17] J. Chem. Educ. 72 (1995) A109.
[18] D.J.M. King, S.T.Y. Cheung, S.A. Humphry-Baker, C. Parkin, A. Couet, M.B. Cortie, G.R. Lumpkin, S.C. Middleburgh, A.J. Knowles, Acta Materialia 166 (2019) 435–446.
[19] E. Burzo, ed., Hydrogen Storage Materials, Springer-Verlag, Berlin Heidelberg, 2018.
[20] V. Dixit, L. van Eijck, J. Huot, Journal of Alloys and Compounds 844 (2020) 156130.
[21] C.-C. Shen, H.-C. Li, Journal of Alloys and Compounds 648 (2015) 534–539.
[22] H. Itoh, H. Arashima, K. Kubo, T. Kabutomori, K. Ohnishi, Journal of Alloys and Compounds 404–406 (2005) 417–420.